ELSEVIER

Catalysis Today 40 (1998) 147–156

CATALYSIS TODAY

# Kinetic study of the water–gas shift reaction and its role in the conversion of methane to syngas over a Pt/MgO catalyst

D. Wolf[1,*], M. Barré-Chassonnery[2], M. Höhenberger, A. van Veen, M. Baerns[1]

*Ruhr-Universität Bochum, Lehrstuhl für Technische Chemie, D-44780 Bochum, Germany*

**Abstract**

Transient as well as steady-state kinetic experiments were applied for the derivation of the reaction mechanism and kinetic constants of the water–gas shift reaction over a Pt/MgO catalyst. Separate investigations on Pt-black and MgO were performed to elucidate the interaction of the metal and support component in the catalytic process. The rate of equilibration of the water–gas shift reaction was compared with the rates of methane conversion to syngas by steam reforming, $CO_2$ reforming and partial oxidation. Among these reactions the water–gas shift reaction is the fastest reaction step. $CO_2$ and $H_2$ adsorbed on MgO, OH-groups on MgO as well as CO adsorbed on Pt should be the reactive surface species. Hence, Pt as well as MgO play an important role in the catalytic process. While MgO provides sites for $CO_2$ adsorption and $H_2$ activation, the formation of stable Pt–CO adsorbates should be the driving force of $CO_2$ dissociation. © 1998 Elsevier Science B.V.

## 1. Introduction

The water–gas shift reaction has to be taken into account as an important and fast reaction step in the conversion of methane to syngas via steam reforming, $CO_2$ reforming or partial oxidation. Among these processes, partial oxidation and $CO_2$ reforming have been extensively studied during the last years as alternatives to the conventional steam reforming process [1]. Supported noble metals with Rh, Ru or Pt as active components have been found to catalyze both the reactions [2]. Commercial scale operation of these reactions involving strong heat effects requires reliable kinetic models. In a complex reaction, as the partial oxidation of methane which is a sequence of a highly exothermal primary reaction (total combustion of methane) and endothermal secondary reactions (steam and $CO_2$ reforming) [2,3], such kinetic models should reflect all significant steps of the reaction mechanism. Against this background, the kinetics of the water–gas shift reaction over a Pt/MgO catalyst, highly active both for oxidation and reforming of methane [3], was studied in a range of reaction temperature which is usually applied for $CO_2$ reforming and partial oxidation of methane. In the derivation of the kinetic-reaction model, no assumption of rate determining surface steps was made. Furthermore, principles of mass action kinetics were taken into account [4] to obtain thermodynamic consistency of the kinetic model. These decisions required detailed information on the reaction mechanism including the surface processes. For this purpose, transient as well as steady-state kinetic data were used to establish the reaction mechanism and to determine adsorption and rate constants as well as adsorption enthalpies and

*Corresponding author. Fax: +49 30 63924454; e-mail: dwolf@aca.fta-berlin.de

[1]Present address: ACA Rudower Chaussee 5, D-12484 Berlin

[2]Present address: Bât 2/appt 925, Place Grand'Goule, 86000 Poitiers, France.


*PII* S0920-5861(98)00003-0

activation energies. Separate investigations on Pt-black and MgO were performed to elucidate the role and the interaction of the metal and support component in the catalytic process.

## 2. Experimental

### 2.1. Catalyst

The Pt(1 wt%)/MgO catalyst was prepared by impregnating the MgO support (Johnson Matthey) with an aqueous solution of $PtCl_4$ (Merk, $c=0.041\ \mathrm{mol\ l^{-1}}$) followed by consecutive drying at 300 K for 24 h and reduction in flowing $H_2$ at 1073 K for 6 h. Besides the Pt/MgO catalyst, also Pt-black (Johnson Matthey) as well as MgO treated in $H_2$ at 1073 K for 6 h were studied.

### 2.2. Kinetic data

#### 2.2.1. Steady state

Steady-state kinetic data of the reverse water–gas shift reaction were measured in a tubular fixed bed reactor made of quartz (ID=6 mm). To determine the temperature in the catalyst bed an alumina well (diameter: 3 mm), for the thermocouple, was inserted into the reactor which was heated by a fluidized sand bed. A high gas velocity (3 m/s) and small-sized catalyst particles (0.25–0.35 mm) were applied to suppress external mass- and heat-transfer limitations during the measurement of kinetic data in the 933–1123 K range. The catalyst mass was varied between 0.01 and 0.20 g resulting in a contact time of 0.06–1.3 ms. The $CO_2$ and $H_2$ partial pressures were varied between 2 and 6 kPa. Nitrogen was used as a balance gas. For gas analysis, a gas chromatograph (Carle 1-111H) equipped with a TC detector and hydrogen-transfer system was applied.

For the kinetic modelling of the partial oxidation of methane, 50 sets of experimental data were available which were obtained by the variation of temperature (six levels), composition of feed gas (eight different ratios of $H_2/CO_2$) and mass of catalyst (five values).

#### 2.2.2. Transient experiments

The interaction of reactant molecules (CO, $CO_2$) with the catalyst surface was investigated by pulsing the gases (ca. $10^{15}$ molecules per pulse) over the catalyst bed which was evacuated before. For this purpose, a temporal-analysis-of-products (TAP) reactor was used. The reactor, the analytical equipment and the procedure of data evaluation is described in more detail elsewhere [5].

## 3. Kinetic modelling

### 3.1. Steady-state data

The reactor was described as an isothermally operating tubular plug-flow reactor. Assuming steady-state conditions for the reaction and the validity of the perfect gas law, the material balance for the gas-phase species ($CO_2$, CO, $H_2$, $H_2O$) is:

$$\frac{\mathrm{d}p_i}{\mathrm{d}(m_{\mathrm{cat}}/V^0)} = RT\sum_j \nu_{ij} r_j. \tag{1}$$

This system of differential equations was integrated numerically by a Gear algorithm [6].

No rate determining reaction step was supposed for the derivation of rate equations. Hence, for the steady state of the reactor the mass balance of the surface species yields a system of non-linear equations since the differential term $\mathrm{d}\theta_i/\mathrm{d}(m_{\mathrm{cat}}/\dot{V}^0)$ must be zero:

$$\frac{\mathrm{d}\theta_i}{\mathrm{d}(m_{\mathrm{cat}}/V^0)} \stackrel{!}{=} 0 = \frac{N_{\mathrm{A}}}{ZA_{\mathrm{BET}}\rho_{\mathrm{cat}}}\sum_j \nu_{ij} r_j = \sum_j \nu_{ij} k_j \left(\prod_m \theta_{mj}^{a_{mj}} \prod_n p_{nj}^{b_{nj}}\right) \tag{2}$$

The steady-state surface coverages $\theta_i$ resulted from the numerical solution of the set of non-linear equations (Eq. (2)) and the balance of normalized surface coverages $\theta_i$ of the Pt and the MgO surface (Eq. (3a,b)):

$$1 = \sum_i \theta_i^{\mathrm{Pt}}, \quad 1 = \sum_i \theta_i^{\mathrm{MgO}} \tag{3a,b}$$

In the kinetic model without assumption of rate determining reaction steps, rate constants were estimated using a numeric strategy introduced by Wolf and Moros (genetic algorithm [7]).

Mass- and heat-transfer limitations could not be fully excluded as the external efficiency factor was estimated to be ≈0.5 on the basis of the measured initial rate of feed consumption. Therefore, a heterogeneous one-dimensional model was used. Mass- and

heat-transfer coefficients were derived on the basis of correlations for small particle sizes and low Reynold numbers [8] corresponding to each experimental situation. Spherical particles were assumed. Values of thermal conductivity and diffusion coefficients were calculated by relationships which were summarized by Kee et al. [9].

It was assumed that the reaction takes place only on the external particle surface. This assumption was supported by the observation that the Pt/MgO catalyst ($S_{BET}$=13 $m^2\ g^{-1}$) is characterized by a low Pt dispersion ($D_{Pt}$=5% measured by CO chemisorption) which corresponds to an average particle size of 24 nm assuming spherical particles. Moreover, TEM analysis showed Pt particles (size: 2–30 nm) at the outer sphere of the catalyst grains implying that the active platinum sites should not be located within the pores and that diffusional limitation can be neglected.

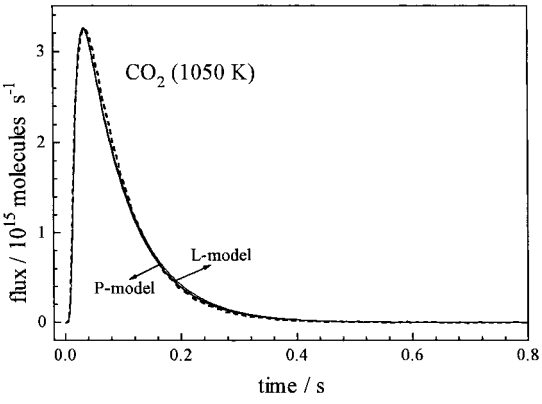


Fig. 1. Comparison between simulated and experimental $CO_2$ response after pulsing $CO_2$ (ca. $10^{15}$ molecules per pulse) over Pt/MgO under vacuum conditions supposing Langmuir adsorption (L-model) or adsorption via a precursor (P-model) (see also Ref. [11]) (· · · experiment, ——— simulation).

### 3.2. Transient data

For the derivation of kinetic constants from transient data a reactor model developed by Rothaemel and Baerns was applied [10]. The procedure of parameter estimation and model discrimination has been reported by Soick et al. [11].

## 4. Results and discussion

To our knowledge, kinetic models and rate constants of the water–gas shift reaction over Pt/MgO catalyst have not been published. Kinetic-rate equations of the Langmuir–Hinshelwood type were reported for $Pt/Al_2O_3$ [12,13] catalysts. However, only low temperatures were considered (<820 K). The studies emphasized a strong effect of the $Al_2O_3$ support on the reaction mechanism including a CO spillover from the metal to the support. These findings indicate that an influence of the support on the reaction, which is expected to proceed on metal sites, is possible for the Pt/MgO catalyst as well.

### 4.1. Mechanism

#### 4.1.1. CO and $CO_2$ adsorption

Adsorption of CO and $CO_2$ on the Pt/MgO catalyst was studied by transient experiments in earlier work. The evaluation of kinetic data has already been reported in Ref. [11]. According to these studies, $CO_2$ adsorption proceeds via formation of a weakly adsorbed precursor and its consecutive transformation into a strongly adsorbed (carbonate or bicarbonate) species. At temperatures above 873 K, the desorption of the precursor becomes much faster than its transformation into the chemisorbed species. Hence, at high temperature, the experimental transient data can be described by a simple Langmuir-adsorption model and the surface coverage by strongly chemisorbed species is negligible (Fig. 1). Since it was shown by other groups that $CO_2$ adsorption on Pt surfaces is extremely weak [14], the $CO_2$ adsorption process on the Pt/MgO catalyst should be determined by the interaction of $CO_2$ with the MgO surface (Table 1: reaction $j$=1).

Two different (weak and strong) adsorption sites of CO on Pt were derived by the previous transient kinetic studies [11] being in agreement with other literature reports [15]. However, at temperatures above 873 K significant adsorption takes place only on those Pt sites which provide the stronger interaction. Adsorption of CO on the MgO surface could generally be neglected within the temperature range investigated (Fig. 2, Table 1: reaction $j$=2).

Table 1
Kinetic model and kinetic parameters of the water–gas shift reaction over Pt/MgO

| Reaction steps | Kinetic rate equation | (Forward) $k_i^{973\,K}$ (mol $Pa^{-1}$ $kg^{-1}$ $s^{-1}$) | (Forward) $E_{A,i}$ (kJ $mol^{-1}$) | (Reversed) $k_{i'}^{973\,K}$ (mol $Pa^{-1}$ $kg^{-1}$ $s^{-1}$) | (Reversed) $E_{A,i'}$ (kJ $mol^{-1}$) |
|---|---|---|---|---|---|
| $CO_2 + [MgO] \underset{j=1'}{\overset{j=1}{\rightleftharpoons}} [MgOCO_2]$ | $r_1 - r_{1'} = k_1 p_{CO_2} \theta_{[]}^{MgO} - k_{1'} \theta_{[CO_2]}^{MgO}$ | $1.2\times10^{25}$ [a] | 0 | $8.5\times10^{28}$ [a] | 241 [a] |
| $CO + [Pt] \underset{j=2'}{\overset{j=2}{\rightleftharpoons}} [PtCO]$ | $r_2 - r_{2'} = k_2 p_{CO} \theta_{[]}^{Pt} - k_{2'} \theta_{[CO]}^{Pt}$ | $7.3\times10^{10}$ [a] | 0 | $7.4\times10^{6}$ [a] | 163 [a] |
| $[MgOO] + H_2 \underset{j=3'}{\overset{j=3}{\rightleftharpoons}} [Mg(OH)_2]$ | $r_3 - r_{3'} = k_3 p_{H_2} \theta_{[O]}^{MgO} - k_{3'} \theta_{[OH]}^{MgO}$ | $4.1\times10^{-9}$ | 47 | $8.5\times10^{-6}$ | 129 |
| $[Mg(OH)_2] \underset{j=4'}{\overset{j=4}{\rightleftharpoons}} [MgO] + H_2O$ | $r_4 - r_{4'} = k_4 \theta_{[OH]}^{MgO} - k_{4'} p_{H_2O} \theta_{[]}^{MgO}$ | $5.0\times10^{10}$ [b] | 82 [b] | $5.5\times10^{25}$ | 0 |
| $[Pt] + [MgOCO_2] \underset{j=5'}{\overset{j=5}{\rightleftharpoons}} [PtCO] + [MgOO]$ | $r_5 - r_{5'} = k_5 \theta_{[]}^{Pt} \theta_{[CO_2]}^{MgO} - k_{5'} \theta_{[CO]}^{Pt} \theta_{[O]}^{MgO}$ | $9.5\times10^{21}$ [c] | 113 | $9.3\times10^{4}$ [c] | 0 |

[a] From transient experiments.
[b] Derived from Eqs. (4) and (5), respectively.
[c] Correlation with the rate constant of the reverse reaction.

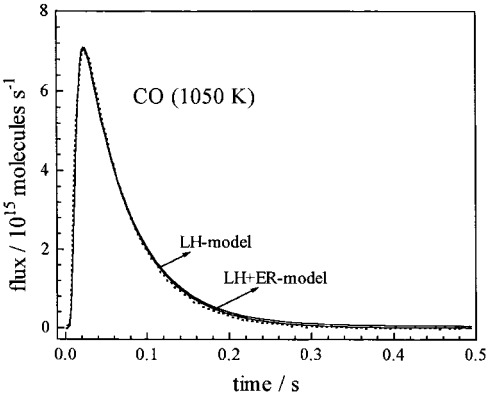


Fig. 2. Comparison between simulated and experimental CO responses after pulsing CO (ca. $10^{15}$ molecules per pulse) over Pt/MgO under vacuum conditions supposing one (LH-model) and two (LH+ER-model) adsorption states of CO (see also Ref. [11]) (· · · experiment, ——— simulation).

### 4.1.2. $H_2$ and $H_2O$ adsorption

$H_2$ and $H_2O$ adsorption were found to be very strong and irreversible under transient conditions. This fact prevented the separate determination of adsorption constants by transient experiments. However, evidence on the interaction of $H_2$ with MgO could be derived in an indirect way from our steady-state kinetic experiments. It was found that the reverse water–gas shift reaction is inhibited by $CO_2$ adsorption on the Pt/MgO catalyst. This was indicated by the dependence of the CO partial pressure at the reactor outlet on the initial $CO_2$ partial pressure at constant $H_2$ partial pressure and contact time (Fig. 3a). (Due to very high catalyst activity the $CO_2$ conversion was already higher than 20% at very low contact time. Therefore, a differential kinetic data analysis, i.e. direct calculation of reaction rates, was not possible.) Since $CO_2$ adsorbs exclusively on MgO sites, the inhibition by $CO_2$ can only be explained if hydrogen adsorbs on MgO sites as well (Table 1: reaction $j$=3). Compared to the $CO_2$ adsorption, the $H_2$ adsorption should be weaker since no drop of the CO partial pressure at the reactor outlet was observed on increasing the $H_2$ partial pressure at the reactor inlet at constant $CO_2$ partial pressure and contact time (Fig. 3b). The adsorption sites could be related to paramagnetic electrophilic oxygen species as $O^-$ or $O_2^-$ on the MgO surface. The existence of such species on MgO and their catalytic activity was reported by Lunsford et al. [16]. As a result hydroxyl groups should be formed which are removed via $H_2O$ formation (Table 1: reaction $j$=4). These findings do not exclude the adsorption of $H_2$ on the Pt surface which is known to occur. However, these adsorbates might be only 'spectators' in the catalytic process.

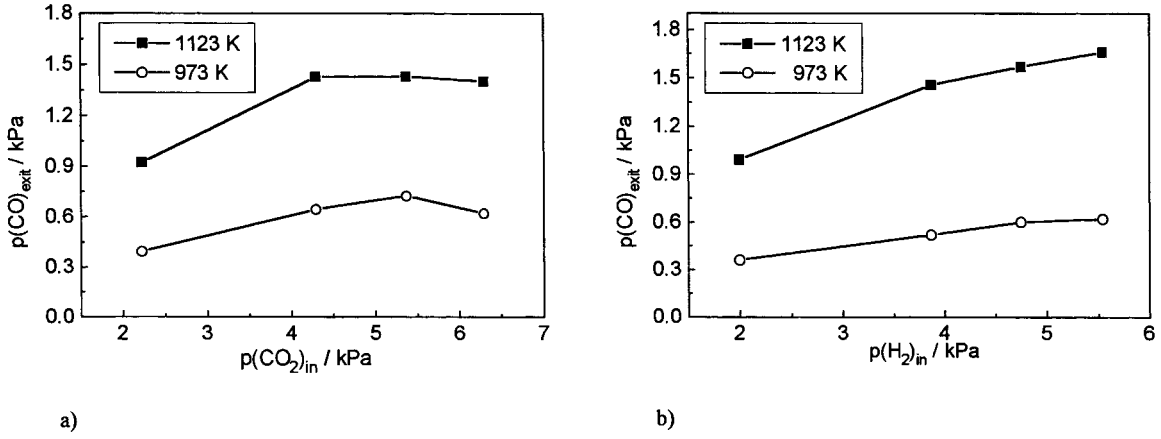


Fig. 3. Dependence of the product formation over the Pt(1 wt%)/MgO catalyst on the partial pressure of reactants at the reactor inlet: (a) variation of $p(CO_2)_{in}$ at constant $p(H_2)_{in}$: $F_{total}$=1 l $min^{-1}$, $m_{cat}$=10 mg, $p(H_2)_{in}$=4.5 kPa; and (b) variation of $p(H_2)_{in}$ at constant $p(CO_2)_{in}$: $F_{total}$=1 l $min^{-1}$, $m_{cat}$=10 mg, $p(CO_2)_{in}$=5.4 kPa.

Table 2
Comparison of the conversion of $CO_2$ by reversed water–gas shift reaction obtained over Pt-black, MgO, a mechanical mixture between Pt and MgO and the Pt(1 wt%)/MgO catalyst ($w/F_{total}$=6 kg s $m^{-3}$, $p(CO_2)_{in}$=5 kPa, $p(H_2)_{in}$=5 kPa)

| Temperature (K) | $X(CO_2)$ (%) Pt-black: $A_{BET}$=11.0 $m^2$ $g^{-1}$ | $X(CO_2)$ (%) MgO: $A_{BET}$=12.8 $m^2$ $g^{-1}$ | $X(CO_2)$ (%) 50 wt% Pt+50 wt% MgO | $X(CO_2)$ (%) Pt(1 wt%)/MgO: $A_{BET}$=13 $m^2$ $g^{-1}$ |
|---|---|---|---|---|
| 1063 | 1 | 2 | 36 | 46 |
| 1093 | 1.5 | 3 | 38 | 48 |
| 1123 | 2 | 5 | 40 | 50 |

#### 4.1.3. *Surface reactions of adsorbed $CO_2$, $H_2$, CO and hydroxyl groups*

Since both $CO_2$ and $H_2$ are adsorbed on the MgO surface, it must be concluded that the reverse water–gas shift reaction occurs on MgO. This assumption was supported by performing the reaction over the MgO support only (cf. Table 2). However, the conversion of $CO_2$ was very low. Compared to MgO the activity of Pt-black was lower, even if the small differences in the surface area are taken into account. If a mechanic mixture of Pt and MgO was used as a catalytic material, a strong increase in the conversion was observed indicating a synergistic effect between the Pt and MgO (Table 2). This synergistic effect has to be discussed also for the Pt(1 wt%)/MgO catalyst. The corresponding additional catalytic driving force might be related to the formation of strongly adsorbed CO species on the Pt surface which favours the dissociation of adsorbed $CO_2$ (Table 1: reaction $j$=5). Hence, the boundary between Pt and MgO appears to provide the active sites for $CO_2$ dissociation. An electrophilic oxygen species is left during this process (Table 1, reaction $j$=5) which may be considered as the active site for hydrogen chemisorption (Table 1: reaction $j$=3).

Thus, the reactions $j$=1 to 5 describe a catalytic cycle of the water–gas shift reaction which explains the inhibiting effect of adsorbed $CO_2$ on the rate of the reversed water–gas shift reaction as well as the synergistic effect between Pt and MgO.

### 4.2. *Rate constants of surface reaction steps*

Adsorption constants and enthalpies of CO and $CO_2$ obtained from former transient studies [11] as well as rate constants obtained by the evaluation of steady-state kinetic data presented here are summarized in Table 1. The rate constants $k_3$, $k_{3'}$, $k_{4'}$, $k_5$, $k_{5'}$ and the corresponding activation energies were obtained by parameter estimation. The thermodynamic consistency of the reaction pathway was warranted since the $k_4$ and $E_{A,4}$ were derived from Eqs. (4) and (5), respectively. Thus, the forward as well as the reversed water–gas shift reaction are described by the kinetic model due to the application of principles of mass action kinetics [4].

$$\prod_j \left(\frac{k^0_{j,\mathrm{rev}}}{k^0_{j,\mathrm{for}}}\right) = e^{\left(\frac{\Delta_R G^0 - \Delta_R H^0}{RT}\right)} \tag{4}$$

$$\sum_j (\sigma_j E_{A,j,\mathrm{for}} - \sigma_j E_{A,j,\mathrm{rev}}) = \Delta_R H^0 \tag{5}$$

Experimental data obtained under steady-state conditions could be described adequately as illustrated by the parity plot of the $CO_2$ partial pressure at the reactor outlet (Fig. 4). Since a single stoichiometric reaction was analyzed all other reactant concentrations resulted from the mass balance. The confidence regions of the

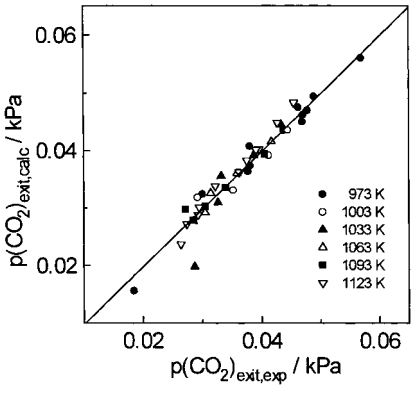


Fig. 4. Parity plot of the $CO_2$ partial pressure at the reactor exit resulting from the kinetic model of the water–gas shift reaction over the Pt(1 wt%)/MgO catalyst.

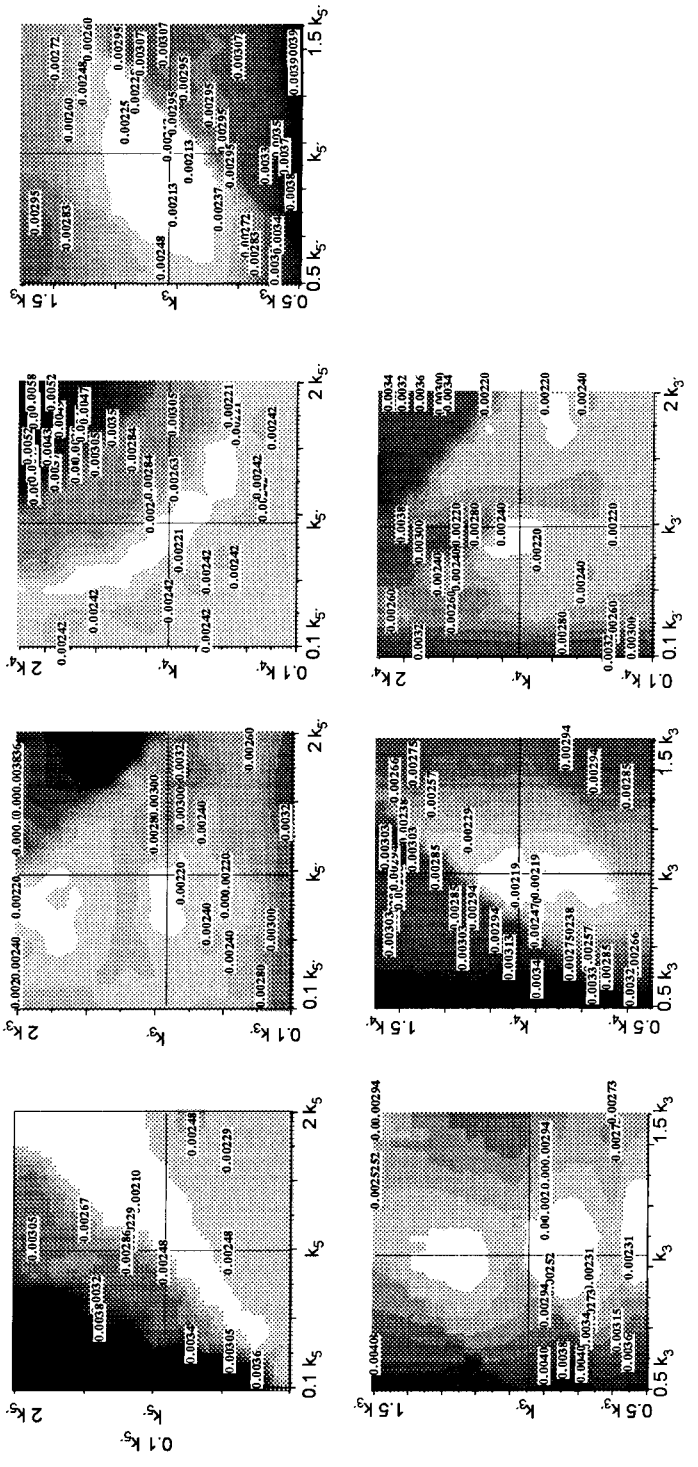

Fig. 5. Pairwise contour plots of the maximum likelihood estimate resulting from the kinetic model of the water–gas shift reaction over the Pt(1 wt%)/MgO catalyst at 973 K.

adjusted rate constants were estimated on the basis of pairwise contour plots of the maximum likelihood estimates according to Bates and Watts [17] (Fig. 5). Linear correlations were found for forward and reversed rate constants $k_5$ and $k_{5'}$. Such linear correlations indicate a very fast equilibration of the corresponding reaction step. In such cases, only the value of the respective equilibrium constant is significant. For the remaining adjusted constants $k_3$, $k_{3'}$ and $k_{4'}$, the contour shapes show closed minimum regions, although strong deviations from elliptical shapes and curvatures due to the non-linearity of the model are observed. Moreover, the existence of more than one local minimum can be derived from the plots $k_{5'}$ vs. $k_{3'}$, $k_3$ vs. $k_{3'}$ and $k_{3'}$ vs. $k_{4'}$. It has to be emphasized, however, that the optimization strategy

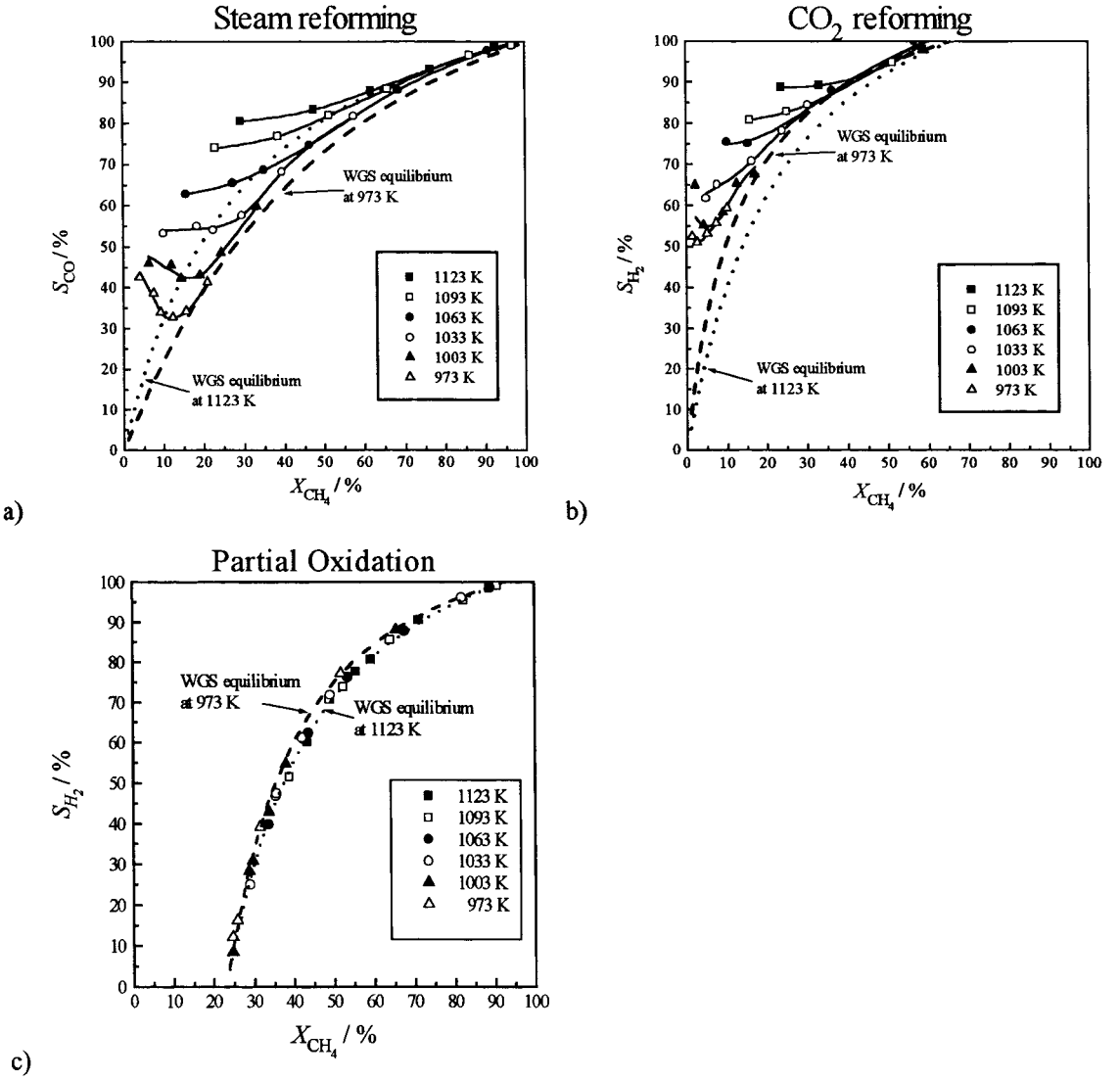


Fig. 6. Dependence of $H_2$ and CO selectivity, respectively, on methane conversion over the Pt(1 wt%)/MgO catalyst: (a) for steam reforming ($F_{total}$=1 l $min^{-1}$, $p(H_2O)_{in}$=3 kPa, $p(CH_4)_{in}$=3 kPa); (b) for $CO_2$ reforming ($F_{total}$=1 l $min^{-1}$, $p(CO_2)_{in}$=2 kPa, $p(CH_4)_{in}$=3 kPa); and (c) for partial oxidation ($F_{total}$=1 l $min^{-1}$, $p(O_2)_{in}$=2 kPa, $p(CH_4)_{in}$=4 kPa).

applied was specially adapted to an efficient global search within very large search regions [7]. Accordingly, a high probability of finding the global optimum was provided.

### 4.3. The role of the water–gas shift reaction in the process of methane conversion

The rate of equilibration of the water–gas shift reaction was compared with that of steam and $CO_2$ reforming as well as with partial oxidation of methane to syngas on the basis of experimental steady-state kinetic data. The dashed and dotted lines in Fig. 6(a, b and c) illustrate the hypothetical product distribution (CO and $H_2$ selectivity) according to the equilibrated water–gas shift reaction at each state of methane conversion. For all three types of reaction, it is evident that the experimental values of CO and $H_2$ selectivities approach the values determined by the water–gas shift equilibrium already at low methane conversion. Hence, the water–gas shift reaction in both directions – forward and reverse – is faster than the methane conversion in any of the reactions under consideration, in particular, at lower temperatures. On increasing reaction temperatures, the methane conversion at which the water–gas shift reaction becomes equilibrated increases as well. This is, most likely, due to the higher activation energies of the reforming and oxidation steps as compared with the water–gas shift reaction.

## 5. Conclusions

The water–gas shift reaction is a very rapid equilibrated reaction step in the methane conversion by steam reforming, $CO_2$ reforming and partial oxidation to syngas over a Pt/MgO catalyst. $CO_2$ and $H_2$ adsorbed on the MgO surface, OH-groups of the MgO surface as well as CO adsorbed on the Pt surface participate in the reaction pathway. A synergistic interaction between Pt and MgO was derived for the reverse water–gas shift reaction which was explained by an additional driving force of the $CO_2$ dissociation due to the formation of stable CO adsorbates on the Pt surface. These findings indicate that the Pt as well as the MgO surface play an important role in the catalytic process of the water–gas shift reaction.

## 6. List of symbols

| | |
|---|---|
| $A_{BET}$ | specific surface area ($m^2\ kg^{-1}$) |
| $E_A$ | activation energy (kJ $mol^{-1}$) |
| $k_j$ | rate constant of the $j$th reaction step (mol $kg^{-1}\ s^{-1}\ Pa^{-b}$) |
| $m_{cat}$ | mass of catalyst (kg) |
| $N_A$ | Avogadro number (number of molecules $mol^{-1}$) |
| $p_i$ | partial pressure of the component $i$ (Pa) |
| $R$ | relative gas constant (J $K^{-1}$ $mol^{-1}$) |
| $r_j$ | rate of the $j$th reaction (mol $kg^{-1}\ s^{-1}$) |
| $S_i$ | selectivity of the component $i$ (%) |
| $S(\vec{k})$ | residual sum of squares function |
| $T$ | temperature (K) |
| $\dot{V}^0$ | total flow rate ($m^3\ s^{-1}$) |
| $X_i$ | conversion of the component $i$ (%) |
| $Z$ | density of active sites on the catalyst surface (sites $m^{-2}$) |
| $\Delta_R G^0$ | standard free reaction energy (kJ $mol^{-1}$) |
| $\Delta_R H^0$ | standard reaction enthalpy (kJ $mol^{-1}$) |
| $\nu_{ij}$ | stoichiometric coefficient of the component $i$ in the $j$th reaction step |
| $\rho_{cat}$ | catalyst porosity (kg $m^{-3}$) |
| $\theta_i$ | normalized surface coverage of the component $i$ |
| $\sigma_j$ | Horiuti stoichiometric number of the $j$th reaction step of a certain reaction pathway (here: single reaction pathway of water–gas shift reaction). |

## Acknowledgements

The work has been funded by the European Union (CONTRACT Nos. ERBCHRXCT 930290 and JOU2-CT92-0073).

## References

[1] M.A. Pena, J.P. Gómez, J.L.G. Fierro, Appl. Catal. A, (1996) 144.
[2] S.C. Tsang, J.B. Claridge, M.L.H. Green, Catal. Today 23 (1995) 3.
[3] M. Baerns, O. Buyevskaya, L. Mleczko, D. Wolf, Stud. Surf. Sci. Catal., in press.
[4] J.A. Dumesic, D.F. Rudd, L.M. Aparicio, J.E. Rekoske, A.A. Trevino, The Mikro Kinetics of Heterogeneous Catalysis, American Chemical Society, Washington DC, 1993.

[5] J.T. Gleaves, J.R. Ebner, T.C. Kuechler, Catal. Rev.-Sci. Eng. 30 (1988) 49.
[6] NAG Fortran Workstation Library, NAG Group Ltd., 1986.
[7] D. Wolf, R. Moros, Chem. Eng. Sci. 52(7) (1997) 1189.
[8] V. Gnielinski, Int. Chem. Eng. 21 (1981) 378.
[9] R.J. Kee, G. Dixon-Lewis, J. Warnatz, M.E. Coltrin, J.A. Miller, Fortran Computer Package for the Evaluation of Gas-Phase Multicomponent Transport Properties, SANDIA REPORT SAND86-8246 UC-401, 1992.
[10] M. Rothaemel, M. Baerns, Ind. Eng. Chem. Res. 35 (1996) 1556.
[11] M. Soick, O. Buyevskaya, M. Höhenberger, D. Wolf, Catal. Today 32 (1996) 163.
[12] D.C. Grenoble, M.M. Estadt, D.F. Ollis, J. Catal. 67 (1981) 90.
[13] C.W. Lam, M.S. Stacey, D.L. Trimm, Chem. Eng. Sci. 36 (1981) 226.
[14] M.H.F. van Tol, A. Gielbert, R.M. Wolf, A. Lie, B.K. Niewenhuys, B.E., Surf. Sci. 287/288 (1993) 201.
[15] R.G. Compton (Ed.), Comprehensive Chemical Kinetics, Vol. 32, Elsevier, Amsterdam, 1991.
[16] M. Iwamoto, J.H. Lunsford, J. Phys. Chem. 84 (1980) 3079.
[17] D.M. Bates, D.G. Watts, Nonlinear Regression analysis and its Application, J. Wiley and Sons, 1988.